REPORT DOCUMENTATION PAGE

AFRL-SR-AR-TR-05-

0073

1. REPORT DATE *(DD-MM-YYYY)*	2. REPORT TYPE	3. DATES COVERED *(From - To)*
	Final Report	01 Jan 2002 - 31 Dec 2004

4. TITLE AND SUBTITLE
Computational Modeling of MEMS Microjets for Turbulent Boundary Layer Control

5a. CONTRACT NUMBER

5b. GRANT NUMBER
F49620-02-1-0093

5c. PROGRAM ELEMENT NUMBER

6. AUTHOR(S)
David B. Goldstein

5d. PROJECT NUMBER

5e. TASK NUMBER

5f. WORK UNIT NUMBER

7. PERFORMING ORGANIZATION NAME(S) AND ADDRESS(ES)
Center for Aeromechanics Research
Department of Aerospace Engineering & Engineering Mechanics
The University of Texas at Austin
Austin TX 78712

8. PERFORMING ORGANIZATION REPORT NUMBER

9. SPONSORING/MONITORING AGENCY NAME(S) AND ADDRESS(ES)
USAF/AFRL
AFOSR
801 N. Randolph Street
Arlington VA 22203

NA

10. SPONSOR/MONITOR'S ACRONYM(S)
AFOSR

11. SPONSOR/MONITOR'S REPORT NUMBER(S)

12. DISTRIBUTION/AVAILABILITY STATEMENT

Distribution Statement A. Approved for public release; distribution is unlimited.

13. SUPPLEMENTARY NOTES

14. ABSTRACT

As a three year continuation of our earlier AFOSR work, we examine novel MEMS actuators for turbulent boundary layer control. The devices of interest are small and closely spaced and hence require detailed direct numerical simulation of the near surface flow to capture the physics. The devices we examine in most detail are arrays of discrete wall-normal jets to test a practical implementation of the opposition control schemes already shown to produce large drag reductions. We alo performed some simple experiments examining pairs of small suction holes used to generate hairpin vortices. While the actuators are examined for their potential application for drag reduction, the emphasis of the work is more on studying the fundamental nature of the flows generated by such devices and how such small scale flows interact with the turbulent vortex structures in a wall-bounded flow. In this final report we emphasize results from simulations of arrays of 3-D slot-jet actuators triggered by practical wall-mounted sensors. Time averaged data show how the jet arrays affect the mean shear stress distribution over the controlled surface while instantaneous data show the interactions of the three-dimensional structures in detail.

15. SUBJECT TERMS

16. SECURITY CLASSIFICATION OF:			17. LIMITATION OF ABSTRACT	18. NUMBER OF PAGES	19a. NAME OF RESPONSIBLE PERSON
a. REPORT	b. ABSTRACT	c. THIS PAGE			19b. TELEPHONE NUMBER *(Include area code)*
U	U	U	UU	16	

Computational Modeling of MEMS Microjets for Turbulent Boundary Layer Control - FINAL REPORT

GRANT NUMBER F49620-02-1-0093

David B. Goldstein

Center for Aeromechanics Research

Department of Aerospace Engineering and Engineering Mechanics

The University of Texas at Austin

Austin, TX 78712
david@cfdlab.ae.utexas.edu

As a three year continuation of our earlier AFOSR work, we examine novel MEMS actuators for turbulent boundary layer control. The devices of interest are small and closely spaced and hence require detailed direct numerical simulation of the near surface flow to capture the physics. The devices we examine in most detail are arrays of discrete wall-normal jets to test a practical implementation of the opposition control schemes already shown to produce large drag reductions. We also performed some simple experiments examining pairs of small suction holes used to generate hairpin vortices. While the actuators are examined for their potential application for drag reduction, the emphasis of the work is more on studying the fundamental nature of the flows generated by such devices and how such small scale flows interact with the turbulent vortex structures in a wall-bounded flow. In this final report we emphasize results from simulations of arrays of 3-D slot-jet actuators triggered by practical wall-mounted sensors. Time averaged data show how the jet arrays affect the mean shear stress distribution over the controlled surface while instantaneous data show the interactions of the three-dimensional structures in detail.

In the following discussion, I summarize and highlight our findings. Further details may be found in the attached papers and MS thesis.

I. Introduction

A turbulent boundary layer is characterized by coherent vortical structures that arise, evolve and decay in a quasi-periodic fashion. The structures, which are dominant in the near-wall region, occupy only 25% of this region but are responsible for approximately 50% of the total turbulence production.[1] Hence, the goal of many researchers and the present research is to actively weaken the coherent structures in the near-wall region to achieve drag reductions over a wall. It is the manipulation of this inner region that interests researchers since it provides the greatest potential for reduction of turbulent energy production. It has been suggested[2] that a quasi-periodic turbulence cycle exists in this near-wall region ($20 < y^+ < 60$) and it is roughly independent of flow away from the wall. Therefore, understanding of the physics of the regeneration cycle is important and some background is briefly described.

Jimenez et al.[2] suggested that the near-wall region is dominated by streamwise velocity streaks superimposed on the mean shear, where the mean shear is maintained by the no-slip boundary condition of the wall. It is well known that streaks can be very long, $x^+ \approx 1000$, have a width of 20 - 40l^*, and have an average spanwise spacing of $z^+ \approx 100$.[3] In addition to streaks, quasi-streamwise vortices dominate the near-wall region; however, because the vortices are not aligned exactly parallel to the wall they only remain in this region for approximately $x^+ \approx 200$.[2] Due to the shorter length of the quasi-streamwise vortices it seems that several vortices can be associated with each velocity streak. This suggests that the physical vortex/streak interaction is crucial for the life of both structures; and in

general, it suggests there are more vortices in the near-wall region than there are velocity streaks. The explanation of how the velocity streaks are created is roughly as follows; as the pairs of quasi-streamwise vortices travel downstream, they tend to pump high momentum fluid (sweep events) towards the wall where low momentum fluid exists due to the no-slip condition of the channel boundaries. In addition, the quasi-streamwise vortices pump low momentum fluid from the near-wall region creating an ejection event of low momentum fluid. The sweep and ejection events result in the alternating streaks of streamwise velocity.

The vertical mixing of the high- and low-momentum fluid helps to create a fuller mean velocity profile characteristic of a turbulent channel flow. The steeper velocity gradient near the channel wall results in a much higher viscous drag than would laminar flow at the same bulk channel velocity.[4] Therefore it is argued that the weakening of the streamwise vortices in the region $20 < y^+ < 60$ may achieve reductions in skin-friction drag. The objective of the current work is the active control of the near-wall region to accomplish drag reduction.

Active control of the turbulent boundary layer has been applied using numerous techniques. The overall objective is the use of small sensors and actuators to provide control based on measurable flow quantities. The progression of research in this area started with physical, intuitive arguments of the boundary layer features but then shifted towards the use of parametric approaches. A brief summary follows describing the numerical and experimental work that has led to the development of the current simulation of turbulent boundary layer control.

A. Numerical Progress in Turbulent Boundary Layer Active Control

Choi et al.[6] use physical intuition in their approach to create a numerical opposition control method. In this method the vertical motion of the near-wall turbulent flow, which is thought of as resulting mostly from the quasi-streamwise vorticity, is sensed at $y^+ \approx 15$ and countered by an equal but opposite blowing/suction distribution velocity on the wall. The technique results in a 25% drag reduction. However, one major drawback of the method is that it requires knowledge of the flow variables within the flow domain. Also, the opposition control is instantaneously applied at every point along the wall throughout the entire channel domain. These drawbacks make the method impractical to physically implement. The work, however, sparked others to develop more practical methods for detection and actuation.

Koumoutsakos et al.[7] sought a numerical feedback control algorithm that uses flow information detected at the wall. The actuating mechanism of this approach is effectively the blowing/suction velocity distribution at the wall, similar to the method of Choi et al.[6] The control scheme is based on the manipulation of the spanwise and streamwise vorticity flux components obtained by measuring the instantaneous pressure at the wall and calculating its gradient. Results using this approach show up to 40% drag reduction for low Reynolds number turbulent channel flow.

Endo et al.[9] developed a numerical feedback control method with an array of sinusoidal deformable wall actuators, roughly $172l^*$ by $60l^*$, to minimize the near-wall coherent structures. When using the opposition control scheme similar to Choi et al.[6] to determine the local wall velocity, the drag is decreased by ~12% with a wall deformation magnitude on the order of $1l^*$. In addition, a second scheme was developed using only wall information. Endo et al.[9] describes the spanwise meandering of the near-wall streamwise streaks as playing an important role in the quasi-cyclic turbulence regeneration process, and he uses the meandering of the streaks to argue that quasi-streamwise vortices accompanied with the meandering streaks can be detected by measuring the streamwise and spanwise gradient of the wall shear stresses. They conclude that by using only wall information they can actuate on quasi-streamwise vortices $50l^*$ downstream from the wall sensors. Yet through their actuation only a 10% drag reduction can be achieved.

In addition to the above applications, research on the control of turbulent boundary layers has made use of control theory to examine the control algorithms. Lee et al.[8] developed a sub-optimal feedback control law that requires pressure or shear stress information at the wall. Using the blowing/suction actuation of Choi et al.,[6] the numerical method was applied using as the detection variables the local gradients of pressure and shear stress in a turbulent channel flow at $R^* = 110$ resulting in a 16 - 22% reduction in skin-friction drag. Of the two detection quantities used by Lee et al.,[8] they found that the spanwise derivative of the spanwise shear at the wall is a slightly better quantity to use as a control input as it results in a 22% reduction in skin-friction drag. In Ref. 10, Lee et al. make use of a neural network based on the spanwise wall shear stresses to activate the blowing/suction velocity distribution at the wall, achieving a 20% reduction of skin-friction. The numerical control scheme detects edges of local high-shear stress regions, which are elongated in the streamwise direction, by measuring the spanwise variation of the spanwise shear stress. Lee et al.[10] investigate how wall shear stresses correlate with wall actuations and make use of a neural network to approximate the correlation which then predicts the optimal wall actuation. They find that the detection of the spanwise shear stress at several points across a spanwise distance of $z^+ = 90$ is enough to achieve good performance of the control algorithm. Furthermore, the correlations suggest that the root-mean-squared value

of the actuation should be approximately $0.15u^*$ for suppression of the near-wall streamwise vortices. But, again, this value is averaged over the whole active wall; there are no discrete actuators.

B. Experimental Progress

Experiments in turbulent boundary layer control are difficult due to the small length and time scales that characterize turbulent flow; the design and fabrication of sensors and actuators is hard.[11] Rathnasingham and Breuer[11] investigate the active control of the near-wall turbulent boundary layer by using the key assumption that the dynamics of the large-scale coherent structures can be described as a linear process for a short period of time. The assumption is based on the observation that the mean shear of the near-wall turbulent flow will dominate during the short time it takes for the flow perturbations to evolve.[12] In addition, it is important to note that the assumption holds only for the time it takes a structure to convect from a sensor to an actuator, and does not imply that turbulence production is a linear mechanism.[19] Using an array of upstream flush-mounted sensors and flush-mounted resonant membrane-type actuators, Rathnasingham and Breuer made a series of experimental observations[1,11] of the boundary layer to provide the optimal transfer functions to predict the downstream characteristics of the streamwise velocity fluctuations. This process predicted, in contrast to the numerical correlations of Lee et al.,[10] that the control jet amplitude should be approximately three times stronger and have root-mean-squared values of area-averaged vertical velocity of $0.45 - 0.55u^*$.[1] The difference in actuation strengths between the two research teams may be due to the fact that the Breuer et al.[1] actuators are discrete jets that do not cover the entire domain and therefore may need stronger actuations locally while the actuation mechanism of Lee et al.[10] is an instantaneous blowing/suction velocity distribution of the entire domain wall. Control results[1] show a maximum reduction of streamwise velocity fluctuations of 30%, with the reduction spanning a region $100l^*$ downstream of the actuator, $50l^*$ in the spanwise direction, and $150l^*$ in the wall normal direction.

An experimental investigation by Lew et al.[13] uses a linear array of MEMS surface shear stress sensors and a micro-machined pneumatic flap actuator to eliminate streak-like regions of high shear stress before their natural dissipation occurs along the channel wall. Open-loop actuation tests show that over an actuation cycle a net reduction of surface shear stress results. It is also found that the reduction is proportional to the actuation amplitude compared to the boundary layer thickness.[13] Furthermore, to ensure interaction with the coherent structure, the actuation amplitude of the flap was limited to $y^+ < 7$ which puts its peak displacement just beyond the viscous sub-layer.

Jacobson et al.[14] develop a piezoelectric cantilever flush-mounted with the wall to investigate active control of transitional and turbulent boundary layers. Actuation is applied by allowing a part of the wetted surface to oscillate in and out of a cavity in the surface. The objective is to demonstrate control of steady and unsteady streamwise vortex disturbances in a laminar boundary layer, with the disturbances acting similar to eddies in the wall region of a turbulent boundary layer. The main idea is to draw fluid into the wall and pump it back out in a controlled manner in order to modify the near-wall flow. Results show that the vortices are localized over the actuator and decay quickly downstream while the associated high- and low-speed streaks remain far downstream of the actuator.[14] Other interesting results of the investigation are the dimensional scales found necessary to implement active control successfully. Jacobson et al.[14] suggests the spanwise dimension of the control module should be of order $20l^*$ and in the streamwise dimension of order $200l^*$.

This review has summarized certain progress made in turbulent boundary layer active control. The goal of the work for this grant has been to use aspects of the successful control techniques discussed above to develop a practical control method using the current numerical scheme[15] to best model a realistic simulation of turbulent flow control. Moreover, the emphasis of the work has been on *better understanding of the physics of the control*, not simply developing a maximally effective scheme. The average length and time scales of the near-wall coherent phenomena appear well documented, as are some appropriate detection methods and dimensions of a successful control algorithm. In particular, the results of Breuer et al.[1] and Lee et al.[10] suggest that the root-mean-squared control jet amplitude should be in the range of $0.15 - 0.55u^*$, with perhaps a tendency toward the stronger actuations if one is modeling discrete actuators versus using a uniform distribution of wall-normal velocity on the domain wall. In addition, a control algorithm should closely model the control modules on the dimensions of those in Rathnasingham et al.,[11] where the sensors used are hot-wires aligned in the streamwise direction and the actuators are narrow in the spanwise dimension ($\sim 10l^*$) and long in the streamwise dimension ($\sim 150l^*$). These dimensions are also roughly the same as those suggested by Jacobson et al.[14] Moreover, the findings of Rathnasingham et al.[11] suggest that the average convection speed of the large-scale structures of turbulent flow is approximately $u^+ = 10.7$. This allows a control algorithm to account for the time between the detection event upstream of the actuators and the actuation event imposed on the structures downstream. Finally, if the control algorithm requires flow variables

measured at the wall only, a good detection scheme to model is that of Lee et al.;[8] this scheme detects the spanwise derivative of the spanwise shear stress at the wall and has been shown to work successfully by Endo et al.[9]

C. Current Turbulent Boundary Layer Control Methodology

Two control schemes shown in Fig. 1 were developed; the first a control algorithm based on the detection methodology of Lee et al.[8,10] and another based on the experiments of Lew et al.[13] An array of discrete wall-normal micro-actuators that act upon oncoming streamwise vortices was modeled.

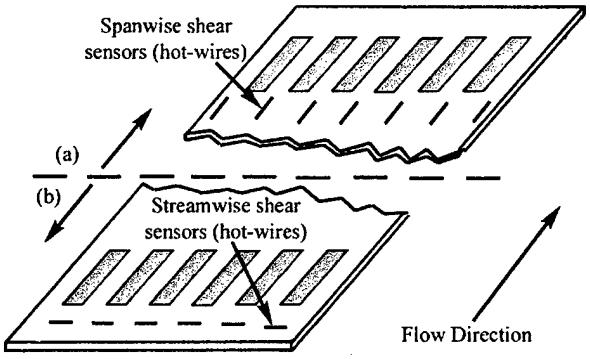

Fig. 1 Schematic of the two current detection schemes. Modeled as hot-wires approximately $2l^*$ above the surface; (a) detection of spanwise gradient of spanwise shear (based on Lee et al.[8, 10]); or (b) detection of regions of high and low streamwise wall shear stress (based on Lew et al.[13]).

Early numerical studies in our group[16] have shown that when continuously operated in a turbulent boundary layer, small MEMS devices can substantially affect structures well beyond the buffer layer but such strong actuation was not found to decrease drag on the surface. Further studies with a single row of actuators[17] show that the physics of flow induced by an array of actuators differs considerably from the idealized case of uniform suction/blowing at the surface as in Koumoutsakos et al.[4] and Choi et al.[6] Yet, the research reviewed in the previous section suggests the potential of discrete actuators in achieving some form of flow control. The use of wall information upstream of individual actuators to detect oncoming streamwise vortices modifies a previous velocity opposition control method in Lee and Goldstein.[17] In that approach, which is based on the opposition control method of Choi et al.,[6] the wall-normal velocity was sensed directly above each actuator slot along a plane $10.6l^*$ above the wall as shown in Fig. 2. An instantaneous response from the slot jets counteracted the detected wall-normal velocity. The objective of the current study is to compare the reduction in drag of the Lee and Goldstein method[17] with the more feasible approach of upstream detection of wall information. A brief discussion of the computational method and domain is followed by a detailed discussion of the results.

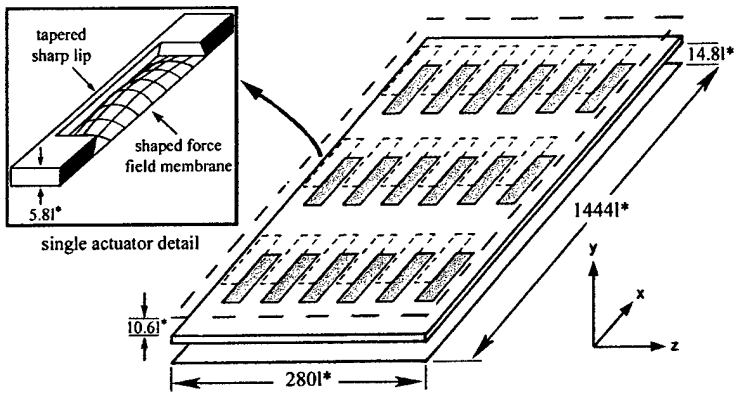

Fig. 2 Schematic of manipulated surface with array of actuators and actuator detail. Sensing regions of Lee and Goldstein[17] (based on the Choi et al.[6] approach) above each slot are indicated with dashed lines. A close-up view of the actuator is shown. This is the same actuator as used in the present work.

II. DNS Method and Computational Domain

The spectral method, initially used by Kim et al.,[18] expands the spatial variables of the incompressible Navier-Stokes equations with Fourier and Chebyshev polynomials. The equations are solved with a Chebyshev-tau method with cosine grid clustering in the wall-normal direction. Time stepping is done with an Adams-Bashforth scheme for the non-linear terms and Crank-Nicholson for the viscous terms. A localized force field similar to the one described by Goldstein et al.[17] is used to simulate stationary and moving boundaries that make up the various parts of the actuators. Please refer to the work of Lee and Goldstein,[16,17,19] as well as the dissertation by Lee[20] for a discussion of the details and issues related to the formulation of the governing equations and code validation and convergence.

The full computational domain consists of a rectangular channel with mean flow in the x-direction. Flow is periodic in both the x and z directions while the horizontal top and bottom y-normal planes are defined as the channel boundaries. The discrete actuator, shown in Fig. 2, is configured to be similar to those tested by Rathnasingham and Breuer[12] and Wu and Breuer.[21] Individual rectangular holes are cut in a raised plate mounted above the lower boundary of the channel. The lips of each slot are tapered to be wider at the membrane location and narrower at the exit plane. The sharp lips are used to promote vortex separation[24] which was thought to be especially useful if modeling jet interactions with the turbulent boundary layer.

The membranes are modeled flush at the bottom of each cutout to make up the driving mechanism of each actuator. Membrane deflection is scaled using a factor, $C_{deflection}$, to match the volumetric displacement of a piston-like motion. That is, a unit displacement input to the membrane results in a larger than unity peak deflection that produces that same amount of ejected fluid as the membrane undergoing a piston-like displacement of one unit. Additionally, while each slot has its own driving mechanism, all slots share a common subsurface cavity that supplies fluid for the pumping/suction action.

For the domain in this study $Re_{channel}$ was about 2,118 while R^* was about 116. For consistency, the friction velocity u^*, viscous length scale l^* and viscous time scale t^* were taken from the opposing top wall of the channel that contained no actuators. Those values were taken as constants and used throughout the study whenever friction properties were needed to normalize data or figures. With these parameters, the computational domain measured $280.2l^*$ in width and $1{,}443.7l^*$ in length. Drag results for a second case examining a slightly higher $Re_{channel}$ of about 2,553 with an R^* of approximately 130 are also reported. For this case the friction velocity, viscous length scale and viscous time scale for an $R^* = 130$ are used. A summary of the relevant flow parameters for the turbulent channel flow is given in Table 1.

Table 1 Summary of relevant flow parameters for the turbulent channel flow

Quantity	R* = 116	R* = 130
Centerline Reynolds number – $Re_{channel}$	~2,118	~2,553
Turbulent Reynolds number – R^*	~116	~130
Friction velocity – u^*	0.03007	0.03350
Viscous length scale – l^*	0.00831	0.00724
Viscous time scale – t^*	0.27635	0.21619
Channel height – 2h	$233.6l^*$	$268.0l^*$
Channel length – L	$1{,}443{,}7l^*$	$1{,}656.6l^*$
Channel width – W	$280.2l^*$	$321.6l^*$
Streamwise resolution – ΔL	$\sim 7.5l^*$	$\sim 8.6l^*$
Spanwise resolution – ΔW	$\sim 1.5l^*$	$\sim 1.7l^*$
Time step – dt	0.0075	0.0075
Number of grid points – x, y, z	128, 64, 128	128, 64, 128

III. Results and Discussion

A. Control Algorithm with Upstream Detection of $\partial\tau_z/\partial z$

1. Overview of Control Algorithm

In this section the results are discussed for the detection methodology which is based on that of Lee et al.[8,10] In particular, the spanwise gradient of the spanwise shear stress is used to detect the near-wall quasi-streamwise vortices upstream of an array of micro-actuators. Here the detailed dimensional information of the control algorithm is given. Using the immersed boundary technique of Goldstein et al.[15] the control module, i.e. the actuator and detection mechanism, is closely modeled after that of Rathnasingham and Breuer.[12] In their study, a pair of hot-wires aligned in the streamwise direction was placed upstream of the actuator to detect the spanwise wall shear stress. By differencing the pair signal, the derivative of the spanwise shear can be approximated. The spanwise spacing between hot-wires is equivalent to the characteristic streak width of $50l^*$. In the current control algorithm such hot-wires are modeled by detecting the spanwise component of velocity at two different points, approximately $2l^*$ above the wall and approximately $47l^*$ apart. Since the detection points are located deep in the viscous sub-layer, measuring the wall shear stress is simply a matter of detecting the velocity component of interest, in the current case it is the spanwise velocity component, and dividing by a constant wall-normal height ($2l^*$). The numerical approximation of the measured quantity used is:

$$\left.\frac{\partial}{\partial z}\left(\frac{\partial w}{\partial y}\right)\right|_{approximated} \cong \left[\frac{w_1}{\Delta y} - \frac{w_2}{\Delta y}\right]\cdot\frac{1}{\Delta z}; \qquad \text{where } \Delta y = 2l^*,\ \Delta z = 47l^* \tag{2}$$

Multiplication by a gain constant, Pamp, of the $\partial\tau_z/\partial z|_{wall}$ and membrane deflection scaling factor yields the opposition blowing/suction magnitude of the actuators.

$$\left(v_{blowing/suction}\right)_{time=t} = (Pamp)\cdot(C_{deflection})\cdot\left[\frac{\partial}{\partial z}\left(\frac{\partial w}{\partial y}\right)\right]_{approximated\ at\ time=t-\Delta t} \tag{3}$$

The dimensions of the actuator, at the surface, are approximately $23l^*$ wide and $143l^*$ long which roughly models the $10l^*$ by $150l^*$ of Ref. 13. The size of the current control module also follows that of Jacobson et al.[14] who suggests control modules of roughly $20l^*$ wide and $200l^*$ in length. The current algorithm is extended into an array of 18 actuators each with a pair of upstream wall shear stress sensors to detect the oncoming streamwise vortices. The array consists of three rows spaced evenly along the streamwise direction. Each row contains six actuators placed

such that the actuators are aligned directly behind each other and have a pitch of approximately $47l^*$. The mean flow is periodic in the streamwise and spanwise directions. In addition, the total cutout area covered by the array of actuators corresponds to 15% of the total surface. The time between the detection event upstream of the actuators and the actuation response is accounted for in the present control method. Using the findings of Rathnasingham and Breuer,[11] which suggest that the average convection speed of the large-scale turbulent structures is approximately $u^+ = 10.7$, and coupled with the finding that quasi-streamwise vortices were successfully detected $50l^*$ upstream of an actuation location by Endo et al.,[9] the current detection points were placed approximately $53l^*$ upstream of the leading edge of the actuator. A delay time variable, Δt, was introduced into the control algorithm to account for the convection time necessary for the detected vortical structure to reach the specified actuator. That time delay is parametrically examined below. Also note that for the $R^* = 130$ case, that the scaled dimensions of the actuator, at the surface, as well as the entire channel domain are approximately 14% larger than those reported above. For an $R^* = 130$ the actuator dimensions using the viscous length scale for this R^*, given in Table 1, are approximately $26l^*$ wide and $164l^*$ long. A general summary of the control system as described above for $R^* = 116$ is shown as a schematic in Fig. 3.

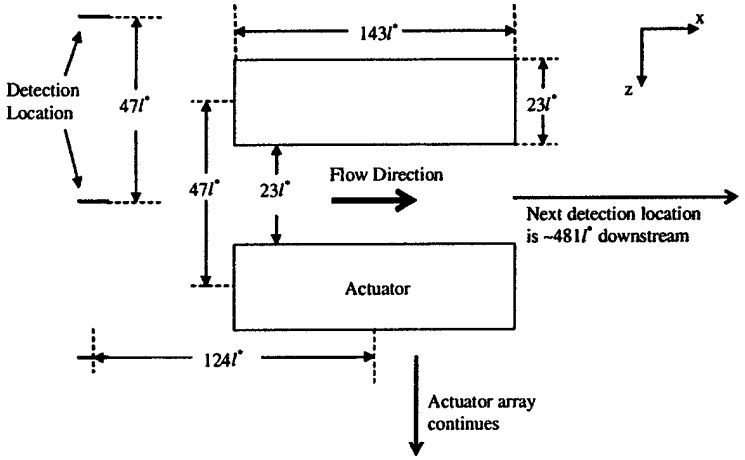

Fig. 3 Summary of detection scheme including spatial dimensions for a portion of the controlled surface for $R^* = 116$. Detection points (modeled as hot-wires aligned in the streamwise direction) are spaced to best sense a streamwise vortex. A time delay variable is introduced into the control algorithm to account for the time it takes a structure to convect the distance from the sensor to the actuator. Length and width of the actuator follow dimensions suggested by Rathnasingham and Breuer[11] and Jacobson et al.[14]

2. Optimal Signal Gain

A study was performed to determine the size of a gain constant, *Pamp*, that sets the strength of the actuating mechanism in Eq. 3. The results of Breuer et al.[1] and Lee et al.[10] suggest that an actuation gain should be applied such that the root-mean-squared control jet amplitude is in the range of $0.15 - 0.55u^*$. Since the current scheme models discrete actuators, a control jet toward the stronger end of this amplitude range was chosen. A brief parametric study of the *Pamp* constant was performed to determine the best value, i.e. the case that resulted in the largest short-term drag reduction. Reported as the drag ratio in the following figures, this parameter is used to quantify the performance of the control algorithm by comparing the shear stresses on the top, un-actuated channel surface and to the total drag on the bottom surface that includes the flow control mechanism. An optimal *Pamp* value was then used in a long-term simulation. Figure 4 displays the range of the actuator gains examined along with the number of time steps of delay. The figure shows the region of near-wall flow stability for various test cases. Stability was determined through the observation of the near-wall flow over the controlled surface during a series of short simulations. The tests showed that if *Pamp* is set too large, above ~0.75, the actuating membranes are forced too hard. This causes near-wall flow instability as well as CFL failure in the more extreme cases. These unstable gains are outside of the green shaded stable region of Fig. 4. As will be discussed shortly, it was found that where the root-mean-square of the control jet amplitude is approximately $0.28u^*$ the drag appeared minimized. This corresponds to a *Pamp* = +0.5, and as shown in Fig. 4, this value of gain is within the stable region for all values of

time delay examined. In the sections that follow the inactive (*Pamp* = 0.0) control case is compared to the active case where *Pamp* is set to +0.5, unless otherwise stated.

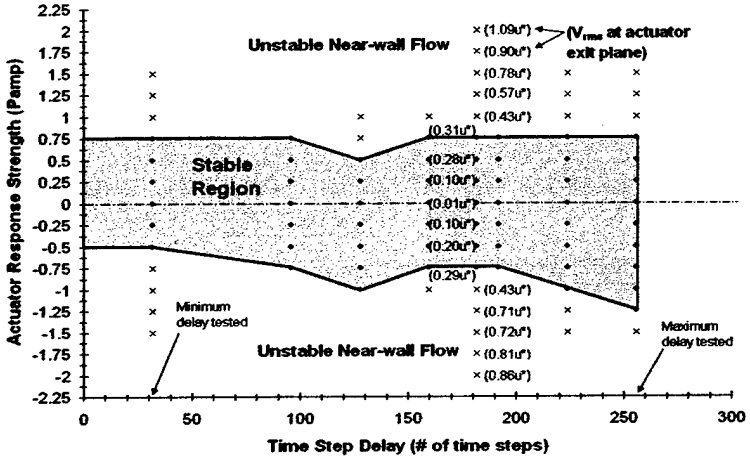

Fig. 4 Stability plot of actuator gain constant, *Pamp*, and time delay, Δt, parametric study. Stability was determined through observation of the near-wall flow over the controlled surface during a short simulation. The stable region is shaded in green and blue dots represent stable test points. Red x's represent test points where the near-wall flow of the controlled surface was visually unstable. V_{rms} data at the actuator exit planes are given in parentheses for a range of *Pamp* values at a time delay of 182 steps.

3. Optimal Time Delay

A brief parametric study is also performed to determine the optimal time delay, or lag, between the detection of the oncoming turbulent structure and the actuation of the sub-surface membrane. This is done by fixing the streamwise distance of the upstream sensors (as seen in Fig. 3) and varying the time delay variable, Δt. It is found that the time delay variations of the study, oddly, have very little effect over a range of $\Delta t = 0.87 - 6.95t^*$. A possible explanation for the lack of a significant effect of Δt is that typical lengths of the velocity streaks can extend up to $1000l^*$ in the streamwise direction[3] which corresponds to time scales of approximately $93t^*$ when assuming $u_c^+ = 10.7$[13] as the average streamwise convection speed of the near-wall turbulent structures. Since the range of the time delay variable used in this parametric study is short compared to the duration of an individual streak it is possible that the range examined is too small and results in no net effect. At first this seems to contradict the study of Rebbeck et al.[25] where they find the control performance to be very sensitive to the phase lag between detection and actuation. However, in that study they detect bursting frequencies which are associated with sweep events. Sweep events are known to be much shorter in streamwise length, typically between $20 - 90l^*$,[3] corresponding to a range of time delay of approximately $2 - 8t^*$. Since the current method seeks to stabilize the near-wall flow with the detection of long low-speed streaks, time delay may have little effect. As a result, the delay is set to $\Delta t = 182$ iterations (or approximately $5t^*$) which is about equal to the convection time of a structure from the detection location to the actuator slot leading edge.

So, what does this control scheme do to the flow? Using these results the next step was to run a longer simulation to 96,000 iterations (or $2605t^*$) to view the long-term effects of the control algorithm on the mean near-wall channel flow.

4. Cross-Sectional Results

The picture may become somewhat more clear if the time-averaged data over the entire simulation duration is examined at a wall-normal height of approximately $y^+ = 2$ as illustrated in Fig. 5. In Fig. 5 a time average of the entire $2606t^*$ of data is taken and the streamwise velocity component is plotted, normalized by the friction velocity. One immediately sees the streamwise acceleration of fluid over each actuator. This is consistent with the notion of altering the no-slip boundary with small portions of a slip-like boundary condition over each recessed cavity.[23]

Moreover, even with the active case, the boundary condition over the individual actuators is slip-like and regions of higher streamwise velocity result. In comparing the two cases, Fig. 5a shows very persistent, long streamwise structures covering the entire length of the domain and spaced approximately $50l^*$ in the spanwise direction. This seems to indicate the presence of the long low-speed streaks characteristic of turbulent wall flow. Of course, they are seen simply because the simulation was not run long enough in this time-averaged data set. Figure 5b shows the active case and one observes how the long streamwise streaky structures are broken up into shorter, thinner structures which extend at most a third of the domain length. This may indicate that small amplitude actuation is enough to break up the long coherent near-wall structures typical of turbulence.

Figure 6 shows the time and spanwise averaged contours of streamwise velocity on the x-z plane located at $y^+ \approx 2$. By averaging in the spanwise direction the long streaks are no longer present and a better view of the flow near the actuators is gained. Streamwise acceleration of the flow is again seen over the actuators. Also notice that beside each actuator is a region of lower speed fluid which occurs as the acceleration of fluid over an actuator slightly entrains the surrounding flow resulting in an inward turning of the velocity streamlines towards the center of the actuator. The spreading streamlines result in a smaller streamwise component of velocity for the regions adjacent to the actuators.

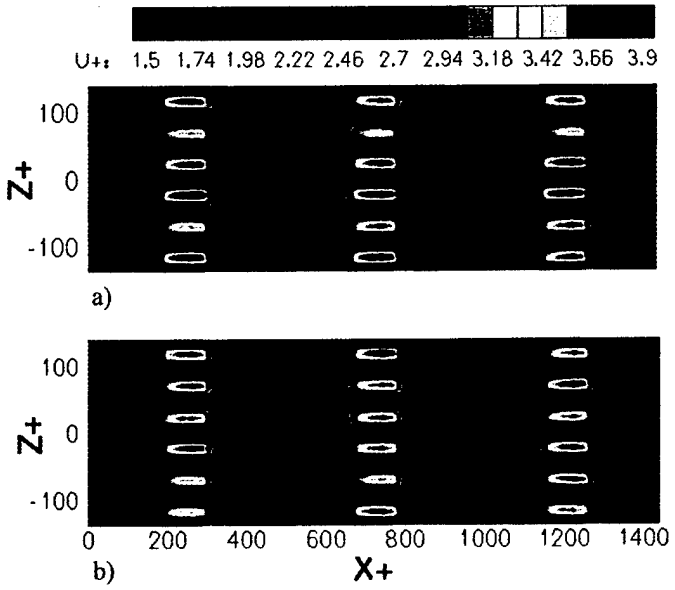

Fig. 5 Time-averaged contours of streamwise velocity on an xz-plane located at $y^+ \approx 2.1$ above the controlled surface for: (a) inactive case (*Pamp* = 0.0) and (b) active case (*Pamp* = 0.5).

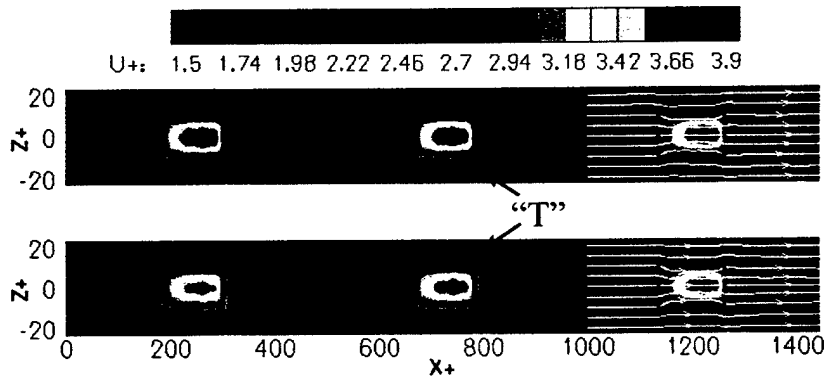

Fig. 6 Time and span-averaged contours of streamwise velocity on an xz-plane located at $y^+ \approx 2.1$ above the controlled surface for: (a) inactive case and (b) active case. Note the stretched z^+ length scale.

Also noticeable is that these low-speed regions seem to be dominant towards the upstream half of the actuators. This may be explained by the dipping of the streamlines into a cavity. The streamlines dip down just aft of the cavity leading edge and entrain the surrounding fluid which causes the deceleration of fluid between actuators. At the downstream end of the cavity the streamlines rise up and out. There, the upward shift in the streamlines compresses the streamlines beside the slot thus producing faster moving fluid surrounding the downstream end of the actuator. This is seen as the characteristic "T" shape of the surface shear stress patterns at the trailing edges of the actuators. A final observation of Fig. 8 is, in the case of active control, the general shortening of the high-speed fluid regions directly downstream of the actuators. This is consistent with regions of reduced shear stress and the overall reduction of skin-friction drag.

More detailed 3-D studies of the effects of actuation on individual turbulent structures are found in the attached documents.

5. Drag Reduction

To quantify the performance of the control algorithms a simple ratio is used to compare the shear stresses on the top, un-actuated channel surface and the total drag on bottom surface that includes the flow control mechanism. This drag ratio is

$$\text{Drag Ratio} = \frac{D_{\text{actuated side}}}{D_{\text{top wall}}} \tag{4}$$

A drag ratio of less then 1 means the control algorithm is working to reduce the skin-friction drag of the manipulated bottom surface. Figure 7a shows the drag ratio trace and running average for the current control algorithm. The figure compares an inactive to an active case. The simulation was run to 96,000 iterations, which is equivalent to $2605t^*$. The running averages of both cases suggest a small drag reduction throughout the duration of the simulation. In general, there seems to be an intermittency period of roughly 15,000 iterations. This period is equivalent to the flow traveling almost three times the length of the domain using the average convection speed of structures at y^+ ~10. The general trend shown in the running average is that, while the initial control resulted in a large drag reduction (~20%), over longer periods of time the control will settle to a very small drag reduction value of just a couple of percent. For the duration of the simulation, active control provides a small drag reduction of 3% ±2.1% whereas the average reduction of the inactive case is 1.2% ±1.4%. Here, the error estimates are calculated by using an autocorrelation of the drag ratio data to determine the length of an independent realization. This realization number is then used to determine the number of statistically independent samples in a data set and the period of these realizations that can be inserted into a statistics program that calculates the standard error.

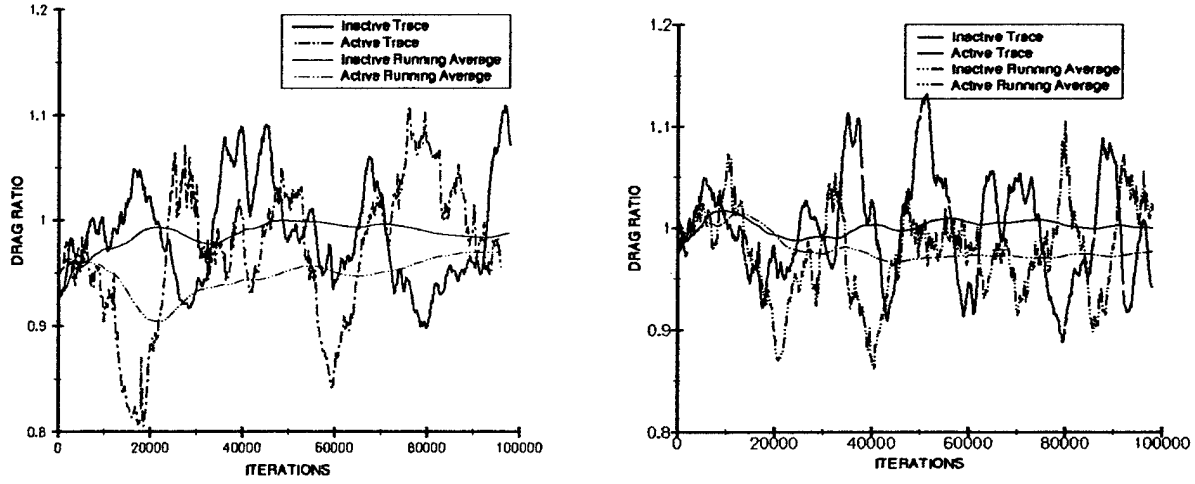

Fig. 7 (a) Drag reductions for the inactive and active cases at $R^* = 116$. Shown is the drag trace and running average for each for time duration of approximately $2606t^*$. (b) Drag trace and running average for the inactive and active cases at $R^* = 130$. Time duration of approximately $3400t^*$.

These results are in good agreement with those of Lee[20] which uses the same immersed boundary layer technique and actuators but a different control methodology of detecting vertical fluctuations over the slots and applying opposition control. In addition, Fig. 7b shows that the results for another active case run at a slightly higher $Re_{channel}$ = 2,552 or R^* = 130 also agree with the first results suggesting that a small increase in the Reynolds Number using the current detection method does not make a significant difference in the drag reduction. In this R^* = 130 case, a small drag reduction of 2.4% ±0.97% was calculated for a *Pamp* of 0.5 and the simulation was run to 98,000 iterations which is equivalent to $3400t^*$. These data are summarized in Table 2. A final note is that Fig. 7a suggests that the running average is still not completely stable at 96,000 iterations which suggests that the simulation has not been run long enough and a simulation out to ~300,000 iterations may be needed to achieve a better statistical average.

Table 2 Average drag reductions for different cases compared to Lee.[20] The number of independent realizations is determined through an auto correlation of the drag.

Case	Indep. Realizations	Average Drag Reduction	Standard Error
Inactive (Pamp = 0.0)	12	1.2%	±1.4%
Active (Pamp = 0.5, R* = 116)	10	3.0%	±2.1%
Active (Pamp = 0.5, R* = 130)	22	2.4%	±1.0%
Inactive, Lee result[20]	10	1.1%	±3.8%
Active, Lee result[20]	38	4.6%	±1.3%

In the next section we investigate a second control algorithm that also utilizes flow information at the wall. The algorithm is easier to comprehend physically as it will target the streamwise component of the high- and low-shear stress regions upstream of the actuators that correspond to sweep and ejection events. Comparison of the two control algorithms may help to confirm that multiple detection quantities can be associated with the coherent near-wall structures and that the use of one over the other may result in larger drag reduction.

B. Control Algorithm with Upstream Detection of $\partial u/\partial y$

1. Overview of Control Algorithm

Here results are presented using a second detection method based on the experiments of Lew et al.[13] The main objective of this scheme is to detect high-and low-streamwise shear stress regions just upstream of a micro-actuator and manipulate the near-wall flow such that the near-wall coherent structures are weakened. In contrast to the previous detection method, the sensors are modeled as hot-wires aligned in the spanwise direction. The streamwise component of velocity is averaged over 16 detection points covering a spanwise width of $23l^*$, equivalent to the width of a single actuator, at approximately $4.51l^*$ above the surface. The height of detection sensors is approximately double that of the previous algorithm in an attempt to avoid the potential detection or amplification of Gibbs phenomena near the edges of the actuator. Furthermore, the boundary condition along the bottom of the computational domain is changed from a no-slip to a slip boundary to ease the Gibbs phenomena. The high- and low- shear regions are determined by comparing an averaged velocity ($u_{avg,\ measured}$) to an optimized mean streamwise velocity. The optimized mean streamwise velocity is taken over the entire actuator plate surface, and is measured as $3.98u^*$. The optimization of this reference velocity is further described in the following section. Equation 5 summarizes the calculation involved in determining whether a high- or low-shear region is approaching an actuator.

$$\frac{u^+_{avg,\ measured}}{u^+\big|_{\substack{\text{optimized mean}\\ \text{over plate surface}}}} - 1 \qquad \begin{cases} > 0 & \text{high-shear region} \\ = 0 & \\ < 0 & \text{low-shear region} \end{cases} \tag{5}$$

$$\left(v_{blowing\,/\,suction}\right)_{time=t} = (\text{Pamp})\cdot\left(C_{deflection}\right)\cdot\left[\frac{\dfrac{u_{avg,measured}}{u^*}}{3.98} - 1\right]_{at\ time=t-\Delta t} \tag{6}$$

Equation 6 shows that a positive value in Eq. 5 will result in a blowing of the actuator in order to deflect away some of the high-speed fluid sweeping towards the wall (therefore $Pamp^{*}C_{deflection} > 0$). Conversely, a negative value in Eq. 5 will direct the actuator to provide suction to a low-speed streak thereby reducing the ejection of this fluid away from the wall, hopefully weakening the streak and perhaps keeping it stable. As shown in Fig. 8, the placement of the sensors is approximately $75l^{*}$ upstream of the actuator leading edge. The actuating mechanism and spacing between actuators remains the same as the previous scheme.

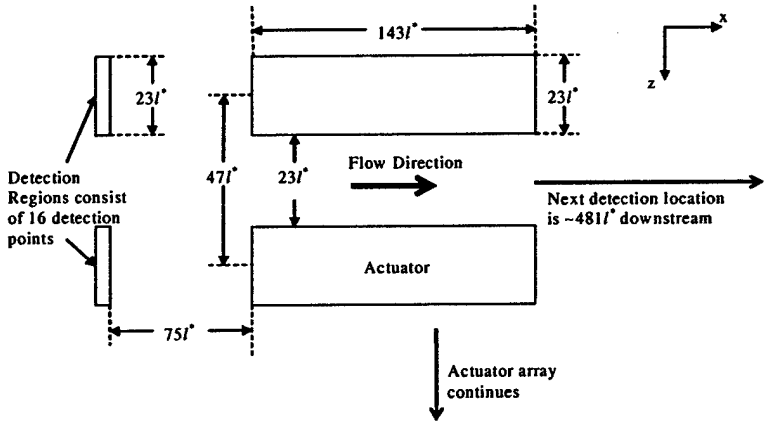

Fig. 8 Summary of spatial dimensions of detection scheme. Shown is only a partial section of the controlled surface. The average over 16 detection points (modeled as a rectangular box hot-wire aligned in the spanwise direction) is used to sense high- and low- shear regions just upstream of an actuator. A time delay variable is introduced into the control algorithm so that the time it takes a structure to convect from the sensor to the center of the actuator ($147l^{*}$) is accounted for. Actuator dimensions follow those suggested by Rathnasingham and Breuer[11] and Jacobson et al.[14]

The next section discusses the optimization of the current control scheme. Specifically, the parameters examined are the time delay and actuator gain signal which are similar to the previous control algorithm. In addition to these two parameters, the optimization of the reference velocity value for the current scheme is examined.

2. *Optimization Process*

Similar to the previous control scheme, an optimization process was attempted to find the test case that presents that greatest drag benefit. Here we discuss the optimization of the mean streamwise velocity over the actuator plate that is selected as our reference velocity in Eq. 5. The quantitative comparison between each local measured streamwise velocity and a reference velocity determines whether approaching flow should be considered a low- or high-speed fluid and therefore this quantity is important to finding a control scheme that works to reduce the drag over the surface. The most obvious idea would be to compare the measured velocity at each wire located at $y^{+} = 4.51$ to the mean x-velocity on the $y^{+} = 4.51$ plane. But it is found that adaptively so choosing the instantaneous mean velocity in a plane a specific height above the actuator surface results in a biased, unstable system. Specifically, the reference value in this case appears consistently too low compared to the measured velocity thereby communicating to the actuator that a high-shear stress region is always approaching the actuators and therefore the actuators try to consistently blow fluid out of the slots. Thus, instead of an instantaneous reference value, a series of fixed reference values were tried including a reference velocity of $4.51u^{*}$, equivalent to the height of the sensor placement above the surface ($4.51l^{*}$), and another reference velocity slightly lower $3.98u^{*}$ obtained by calculating the mean streamwise velocity three grid planes above the surface. In brief simulations of 7000 time steps with a nominal range of *Pamp* values and a $\Delta t = 382$, both velocity reference values produce a stable response unlike the adaptive test case and both give similar drag results. However, using $3.98u^{*}$ as the reference velocity produces a slightly better drag benefit. Therefore, based on this short simulation, a reference velocity of $3.98u^{*}$ is chosen and discussion of the appropriate time delay and signal gain follows.

A series of time delays and actuator signal gains are used to determine the best test case for achieving an overall drag reduction. Three time delays are chosen which correspond to the time it takes the fluid to convect at a

speed of $10.7u^*$ from the upstream sensors to three positions;[11] to the actuator leading edge, to 1/4th the actuator length, and to 1/2 the actuator length. More extreme cases of early actuation and delayed actuation are not investigated to save on computation time in the optimization process. However, a complete range of actuator signal gains (*Pamp*) was tested which cover similar actuation strengths to those used in the previous control scheme. Figure 9 gives an overall view of the various test cases included in the parametric study.

One observes from Fig.9, and by comparing the drag ratio vs. time plots, that varying the time delay parameter has no major affect on the effectiveness of the control scheme. This was also seen in the control scheme based on spanwise shear gradients and is most likely explained by the natural streamwise low-speed velocity streak lengths involved in near-wall channel flow. These streaks can extend up to approximately $1000l^*$, $O(10x)$ the length of our sensor to actuator distance.

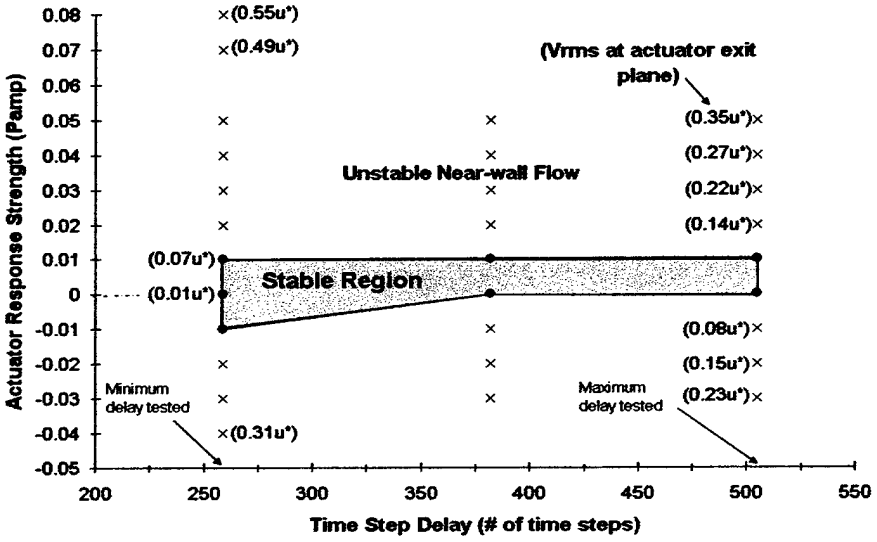

Fig. 9 Plot of actuator gain constant, *Pamp*, and time delay, Δt, parametric test matrix. Stability of the near-wall flow was determined through observation of the near-wall flow over the controlled surface during a short simulation. The stable region is shaded in green and blue dots represent stable test points. Red x's represent test points where the near-wall flow of the controlled surface was visually unstable. V_{rms} data at the actuator exit plane is given for the entire range of *Pamp* in the test matrix.

Results of the parametric study show that in a simulation of 54,000 iterations, equivalent to $1466t^*$, the optimal time delay is $\Delta t = 259$ iterations. This delay is equivalent to the time it takes the flow to travel, assuming $u_c^+ = 10.7$,[11] from the detection sensors to the leading edge of the actuator. A very small $Pamp = 0.01$ is the optimal case among those examined. Such a small value of *Pamp*, of course, produces a very small $v_{rms} \approx 0.07u^*$ at the slot exit plane.

3. Drag Reduction

Results of the streamwise shear stress control method are given by calculating the drag ratio for the current optimal values of $Pamp = 0.01$ and $\Delta t = 259$. In a simulation of 96,000 iterations, the current algorithm results in an average drag *increase* of 8.4% ±2.9%. However, the inactive test case ($Pamp = 0.0$) provides results that do compare to those of the previous control algorithm -- an average drag *increase* of 1.2% ±1.4%, but this barely falls within previous simulation results when including the error bars. Direct comparison with the previous control results and the data of Lee[20] can be made by referring to Table 3.

These results suggest that either the true optimized settings are not yet determined or that this algorithm does not work. Before deciding that this algorithm is ineffective we need to first look at the optimization process used to obtain the reference velocity in Eq. 5. While a series of fixed values were tested, these test cases may not have been

run long enough to provide a clear indication of a stable, working system. Choosing $3.98u^*$ as the optimal reference value for Eq. 5 may have simply contributed to a *slow* drift in the detection data. This subject needs further work.

Table 3 Average drag reductions for preliminary test run

Case	Indep. Realizations	Average Drag Reduction*	Standard Error
Inactive (Pamp = 0.0)	15	-1.2%	±1.4%
Active (Pamp = 0.01)	8	-8.4%	±2.9%

* a negative number indicates a drag increase.

IV. Conclusions

The objective of this paper was to study the physics of a physically realizable device having physically realistic control algorithms based on previous numerical and experimental work in the field. A control design was aimed at producing small disturbances very close to the control surface with the goal of quieting the near-wall vortical structures responsible for the regeneration and maintenance of turbulence. As a result, two control algorithms were examined, both based on detection of a quantity at the wall. The first method used detection of $\partial/\partial z(\partial w/\partial y)|_{wall}$. In addition, results of a second control scheme using the detection of $(\partial u/\partial y)|_{wall}$ were examined. Results after 96,000 iterations using control based on the detection of $\partial/\partial z(\partial w/\partial y)|_{wall}$, show a small 3% ±2.1% reduction in drag with actuation turned on while a smaller 1.2% ±1.4% reduction was observed for the inactive actuators. Results using this same detection, but at a slightly higher R^* of 130, show that after 98,000 iterations a 2.4% ±1.0% reduction in drag was observed. Both of these results are comparable to the reductions of similar test cases produced by Lee[23] whose objective was to dampen the velocity fluctuations just above an actuator by sampling v-velocity at a detection area above each actuator, but well within the flow, and apply a continuous blowing/suction to achieve v-velocity fluctuation dampening in these regions. Both control designs, that of Lee[20] and our method of detecting $\partial/\partial z(\partial w/\partial y)|_{wall}$, cover approximately 15% of the total flat surface by using an array of 18 actuators evenly spaced in three rows on the control surface. The small percentage of control surface covered by actuators explains, in part, why the drag reductions achieved in both control designs are small compared to the ~25% drag reductions reported by Choi et al.[6] whose control dampened the v-velocity fluctuations at every grid point on a detection plane over the entire channel surface. Therefore, if the array of actuators used herein was expanded such that the total control surface was covered, the drag reductions reported here may be approximately 6.5 times larger, a reduction comparable to that of Choi et al.[6] Of course, such a device could then not be built.

A series of parametric studies was performed to obtain an optimal actuation gain and the optimal time delay between the detection and actuation events. It was found that an actuation gain which resulted in $v_{rms} \approx 0.28u^*$ in the slot plane provided the greatest drag reduction over a series of short-term tests. This value falls within the root-mean-squared control jet amplitude range of 0.15 - $0.55u^*$ found in tests by Breuer et al.[1] and Lee et al.[10] However, one should note that the goal of the current work was not to utilize a synthetic jet for opposition control, but to instead use very small flow perturbations in and out of an array of actuators to reduce the drag over a surface. In addition, the optimal time delay, or lag, between detection and actuation events was found to be, surprisingly, not very important for the current control method. This may be due to the typical lengths of the velocity streaks compared to the small range of delays examined. Therefore, a delay corresponding to the time it takes a large scale turbulent structure to convect in the streamwise direction, at an average speed of $10.7u^*$,[11] from the detection location to the leading portion of the actuator was satisfactory.

In addition, results were reported using the second control method which detected a $(\partial u/\partial y)|_{wall}$ quantity at the wall. Actuation resulting in $v_{rms} \approx 0.07u^*$ (for *Pamp* = 0.01) with a time delay to match the convection of the detected structure to the leading edge of the actuator (Δt = 259) were used to gather the data. The potential for drag reduction using this method, surprisingly, does not match that of the first control method examined. With a 8.4% ±2.9% drag *increase* for the active test case, it seems that the $(\partial u/\partial y)|_{wall}$ control is not effective as implemented. These results were achieved using the current parameters believed to be optimal at the time of the simulation. However, choosing $3.98u^*$ as the optimal reference value may have simply contributed to a *slow* drift in the detection data, causing an eventual bias towards either suction or blowing of the array of actuators. Further investigation into this optimal reference velocity parameter is needed before general conclusions about the $(\partial u/\partial y)|_{wall}$ control's effectiveness can be made.

In conclusion, the current research supports the idea of weakening the near-wall coherent structures of turbulent channel flow through the use of physically practical control devices and algorithms which make use of

flow information on the wall. While the reductions reported seem small compared to other the numerical studies, it should be kept in mind that only 15% of the total surface was covered with actuators in the current cases. Furthermore, by increasing the actuator population density somewhat, which is feasible with current progress in MEMS technology, the potential for a significant drag reduction over a surface remains promising.

Publications and Presentations During Period of the Grant

1. Lee, C. Y. and Goldstein, D. B., "Two-Dimensional Synthetic Jet Simulation," *AIAA Journal*, Vo. 40, No. 3, March 2002 (but supported by the previous grant).
2. Lee, C. and Goldstein, D. B., "Simulation of MEMS Suction and Blowing for Turbulent Boundary Layer Control," AIAA Paper 2002-2831, AIAA Flow Control Conference, St. Louis, MO, June 2002.
3. Goldstein, D. B., "Computational Modeling of MEMS Microjets for Turbulent Boundary Layer Control," Lecture and abstract for the AFOSR Contractors' Meeting in Turbulence and Rotating Flows, Ft. Worth, TX, August 2002.
4. Goldstein, D. B., "Computational Modeling of MEMS Microjets for Turbulent Boundary Layer Control," Lecture and abstract for the AFOSR Contractors' Meeting in Turbulence and Rotating Flows, August 2003.
5. Lee, C., Colmenero, G., Goldstein, D. B., Wu, K., and Breuer, K., "Micro-actuators for Turbulent Boundary Layer Control," Lecture presented at the American Physical Society, Division of Fluid Dynamics Meeting, AR5, November, 2003.
6. Colmenero, G., and Goldstein, D. B., and "Turbulent boundary layer control using wall information," AIAA Paper No. 2004-2116, AIAA Flow Control Meeting, Summer 2004.
7. Goldstein, D. B., "Turbulent Boundary Layer Control with Discrete Actuators Using Wall Information," Lecture and abstract for the AFOSR Turbulence and Rotating Flows Conference Report, Denver, CO, August 2004.

Doctoral Dissertation Completed

Lee, Conrad, Y., "Direct Numerical Simulation of Microjets for Turbulent Boundary Layer Control," Summer 2004. Dr. Lee is a Laboratory Research Fellow at UT Austin.

Masters Degree Completed

Colmenero, Gerardo, "Turbulent Boundary Layer Control with Discrete Actuators Using Wall Information," Dec. 2004. Mr. Colmenero will join the US Navy in Spring, 2005.

References

[1]Breuer, K. S., Amonlirdviman, K., and Rathnasingham, R. "Adaptive Feed Forward Control of Turbulent Boundary Layers," AIAA paper 98-1025, 1998.

[2]Jimenez, J. and Pinelli, A., "The autonomous cycle of near-wall turbulence," *Journal of Fluid Mechanics*, 1999, **389**:335-359.

[3]Panton, R., Self-Sustaining Mechanisms of Wall Turbulence, Computational Mechanics Publications, 1997, Chap. 2, 10.

[4]Koumoutsakos, P., Bewley, P., Hammond, E. P., and Moin, P., "Feedback Algorithms for Turbulence Control – Some Recent Developments," AIAA paper 97-2008, 1997.

[5]Goldstein, D. B. and Tuan, T.-C., "Secondary flow induced by riblets," *Journal of Fluid Mechanics*, 1998, **363**:115-151.

[6]Choi, H., Moin, P., and Kim, J., "Active Turbulence Control for Drag Reduction in Wall-Bounded Flows," *Journal of Fluid Mechanics*, 1994, **262**:75-110.

[7]Koumoutsakos, P., "Vorticity flux control for a turbulent channel flow," *Physics of Fluids*, 1999, **11**, No. 2:248-250.

[8]Lee, C., Kim, J., and Choi, H., "Suboptimal control of turbulent channel flow for drag reduction," *Journal of Fluid Mechanics*, 1998, **358**:245-258.

[9]Endo, T., Kasagi, N., and Suzuki, Y., "Feedback control of wall turbulence with wall deformation," *International Journal of Heat and Fluid Flow*, 2000, **21**:568-575.

[10]Lee, C., Kim, J., Babcock, D., and Goodman, R., "Application of neural networks to turbulence control for drag reduction," *Physics of Fluids*, 1997, **9**, No. 6:1740-1747.

[11]Rathnasingham, R. and Breuer, K. S., "System Identification and Active Control of a Turbulent Boundary Layer," AIAA paper 97-1793, 1997.

[12]Rathnasingham, R. and Breuer, K. S., "Closed-Loop Control of Turbulent Boundary Layers," *Unpublished*, Division of Engineering, Brown University, Providence, RI, 2002.

[13]Lew, J., Huang, A., Ho, C-M., Jiang, F., and Tai, Y. C., "Surface Shear Stress Reduction with MEMS Sensors/Actuator in Turbulent Boundary Layers," *Unpublished*, Univ. of California, Los Angeles and Caltech.

[14]Jacobson, S. A., and Reynolds, W. C., "Active control of streamwise vortices and streaks in boundary layers," *Journal of Fluid Mechanics*, 1998, **360**:179-211.

[15]Goldstein, D. B., Handler, R., and Sirovich, L., "Modeling a no-slip flow boundary with an external force field," *Journal of Computational Physics*, 1995, **105**:354-366.

[16]Lee, C. and Goldstein, D. B., "DNS of Microjets for Turbulent Boundary Layer Control," AIAA paper 2001-1013, 2001.

[17]Lee, C. and Goldstein, D. B., "Simulation of MEMS Suction and Blowing for Turbulent Boundary Layer Control," AIAA paper 2002-2831, 2002.

[18]Kim, J., Moin, P., and Moser, R., "Turbulence statistics in fully developed channel flow at low Reynolds number," *Journal of Fluid Mechanics*, 1987, **177**:133-166.

[19]Lee, C. Y. and Goldstein, D. B., "Two-Dimensional Synthetic Jet Simulation," *AIAA Journal*, **40.3**:510-516.

[20]Lee, C. Y., "Direct Numerical Simulation of Microjets for Turbulent Boundary Layer Control," Ph.D. Dissertation, Dept. of Aerospace Engineering, Univ. of Texas at Austin, Austin, TX, 2004.

[21]Wu, K. E. and Breuer, K. S., "Dynamics of Synthetic Jet Actuator Arrays for Flow Control," AIAA paper 2003-4257, 2003.

[22]Rebbeck, H. and Choi, K-S., "Opposition control of near-wall turbulence with a piston-type actuator," *Physics of Fluids*, 2001, **13**, No. 8:2142-2145.